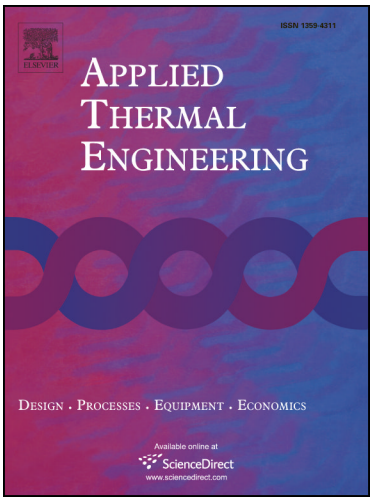


Research Paper

# Adsorption heat pump optimization by experimental design and response surface methodology

Joana M. Pinheiro, Sérgio Salústio, Anabela A. Valente, Carlos M. Silva

PII: S1359-4311(17)35121-9
DOI: https://doi.org/10.1016/j.applthermaleng.2018.03.091
Reference: ATE 11979

To appear in: *Applied Thermal Engineering*

Received Date: 3 August 2017
Revised Date: 14 February 2018
Accepted Date: 27 March 2018

Please cite this article as: J.M. Pinheiro, S. Salústio, A.A. Valente, C.M. Silva, Adsorption heat pump optimization by experimental design and response surface methodology, *Applied Thermal Engineering* (2018), doi: https://doi.org/10.1016/j.applthermaleng.2018.03.091

# Adsorption heat pump optimization by experimental design and response surface methodology

Joana M. Pinheiro[a], Sérgio Salústio[b], Anabela A. Valente[a,*], Carlos M. Silva[a,*]

[a] CICECO - Aveiro Institute of Materials, Department of Chemistry, University of Aveiro, 3810-193 Aveiro, Portugal

[b] Department of R&D of Bosch Thermotechnology, Cacia-Aveiro, 3800-533, Portugal

* *Corresponding authors*. Carlos Manuel Silva: Tel.: +351 234 401 549; fax: +351 234 370 084; carlos.manuel@ua.pt. Anabela A. Valente: Tel.: +351 234 370 603; fax: +351 234 370 084; atav@ua.pt.

**Abstract**

The performance of commercial zeolites, with and without binder in its formulation (SYLOBEAD® MS C 548: 13X with binder; Köstrolith® 13XBFK and NaYBFK: 13X and NaY without binder, respectively), for water adsorption heating applications was compared in this work. Accounting for a Box-Behnken design with four factors (time of adsorption and desorption, $t_{\mathrm{ADS+DES}}$; condensation temperature, $T_{\mathrm{cond}}$; heat source temperature, $T_{\mathrm{HTF,hot}}$; bed thickness, $\delta$) and three levels, a set of 25 simulations per adsorbent was accomplished, and the performance of the adsorption units was evaluated through the coefficient of performance (*COP*) and the specific heating power (*SHP*). The results suggested that the presence of the binder in the formulation of 13X does not penalize the zeolite performance significantly, and that NaYBFK is the most promising material. For the latter solid, statistical outcomes were analyzed and insights about their usefulness to optimize the design and operation of adsorption heat pumps are provided. Pareto charts displaying the impact ranking of the factors upon *COP* and *SHP* are discussed, and simple equations are provided for the expeditious estimation of both indicators. Such models were utilized to map system performance and to select optimal geometric/operating parameters that meet specific performance requirements.

*Keywords*: adsorption heating application, experimental design, optimization, simulation, zeolites

## 1. Introduction

The increasing energy global demands, the dependency of modern society on fossil fuels and the need for reducing greenhouse gas emissions and ozone depletion have motivated the development of eco-friendly technologies based on renewable sources or powered by waste energy [1, 2]. Worldwide energy consumption for heating purposes in the building sector represents a significant portion of energy demands. In residential and commercial buildings, respectively, space heating accounts for 32 % and 33 % of the total energy use, while domestic hot water consumption represents 24 % and 12 % [3]. It is important to develop cost-effective technologies, allying energetic and environmental sustainability with market needs and human comfort. Focus has been put on cooling/heating technologies based on adsorption [4, 5] for the potential replacement of conventional vapour-compression systems (VCS), avoiding the negative impact of fluorocarbon type refrigerants through the usage of eco-friendly fluids such as water. Additionally, adsorption-based systems may be powered by renewable energy sources such as solar energy or waste heat (conversely, VCS use electricity), and present no noise nor vibration problems [2, 6, 7].

Adsorption cooling/heating systems, specifically adsorption heat pumps (AHPs), consist of four main units: an adsorbent heat exchanger (AHEx), condenser, evaporator and expansion valve [8]. The operating cycle of AHPs involves four stages: isobaric adsorption, isosteric heating, isobaric desorption and isosteric cooling [6, 9]. The efficiency and cost-effectiveness of AHPs are strongly influenced by the performance of the adsorbent/adsorbate working pairs. Several studies regarding the analysis of pairs for AHPs have been reported in the literature. For example, Boman *et al.* [10] analysed approximately eighty pairs for heating applications, namely activated carbons with alcohols or ammonia as adsorbates, and MOFs/alcohols. Frazzica and Freni [11]

investigated working pairs for solar thermal energy storage such as zeolite 13X/water, composites of multi-wall carbon nanotubes and LiCl for adsorption of water and methanol, and silica-alumina phosphate AQSOA® FAM-Z02/water, and concluded that the latter two pairs were promising for heating applications. Freni *et al.* [12] identified potential adsorbents using water as adsorbate and compared their heating performances, namely the composite LiBr-silica, silica-alumina phosphates SAPO-34 and AQSOA® FAM-Z02, and standard commercial zeolite 4A, and obtained higher COPs for the composite and silica-alumina phosphates. The investigation of the composite adsorbents is essentially in an academic scope, which hinders the industrialization of AHPs incorporating these materials in the short to medium term. Regarding silica-alumina phosphates, a general issue is the high costs of the synthesis process in relation to standard commercial zeolites, and has not reached production in relatively large scale [12]. On the other hand, zeolites (crystalline microporous aluminosilicates) such as 4A and 13X are cheaper and widely available in the market, albeit their use in AHPs requires demanding regeneration conditions [12]. Zeolites are often commercialized as binder based granules, but the binder introduces passive mass in the AHEx, may reduce the adsorption capacity and hinder intraparticle mass transfer [13]. Aiming at materials with improved performances, the company Chemiewerk Bad Köstritz GmbH (CWK) developed binderless formulated zeolites of the type NaX, NaA and more recently NaY for thermochemical energy storage applications [14, 15], which exhibit improved water adsorption capacity and kinetics in comparison to conventional zeolite beads [13, 16]. Particularly, NaY zeolite presents a higher molar ratio Si/Al than NaX, which contributes to facilitated regeneration of the adsorbent [17].

In order to compete with VCS, AHPs require improvements in terms of coefficient of performance (*COP*), power per unit mass of adsorbent (specific heating power, *SHP*)

and/or per unit AHEx volume (*VSHP*), and costs, as they are still too big and heavy appliances [18, 19]. Research and development priorities have been identified, which include novel adsorbents, compact AHEx designs, and advanced control strategies allowing the system to adapt to changes in operating conditions and user requirements [19]. The performance of AHPs is strongly dependent on the operating conditions (e.g. cycle time, temperatures of condensation and adsorbent regeneration) and geometric factors (e.g. adsorbent configuration - coatings or loose grains - and bed thickness) [6, 20-24]. The cycle time, for instance, may impact conversely on *COP* and power [25-27], which turns it an important optimization parameter. Nonetheless, the study of AHPs is difficult due to the high complexity of the heat, mass and momentum transfer phenomena occurring simultaneously in the adsorbent bed [28], and to the challenging optimization of the system to fit variable working conditions or thermal demands [29].

The optimization of the AHP's design and operation can be performed using phenomenological models (usually coupled with complex numerical optimization tools) [28-35], experimental setups/prototypes [18, 36-39] or a combination of both [40, 41], which may often become a difficult and lengthy task. Specifically, (i) it may be very time consuming, since a significant number of experiments or delayed simulations may be necessary to determine optimal parameters in a broad range of conditions; (ii) it may be very complex or even impossible to identify optimal combinations of operating/geometric parameters to meet pre-established performance requisites; (iii) assessing the impact ranking of several parameters on the performance may not be straightforward. In this regard, statistical methodologies can be combined with phenomenological modeling or experiments in order to perform optimizations much more easily and efficiently.

The design of experiments (DoE) and response surface methodology (RSM) are powerful statistical tools to help identify the main factors and interactions influencing key indicators of a process and for performing expeditious optimizations [7, 42]. These tools are versatile and have been used in distinct fields, allowing a considerable reduction of the number of experiments or simulations required for establishing optimal conditions; e.g. chromatography [43], supercritical fluid extraction [44], coagulation-ultrafiltration for drinking water treatment [45], and synthesis of materials [46]. Despite the great potential of these methodologies, very few studies were related to adsorption-based technologies (and aimed specifically at cooling applications) [7, 8, 42, 47].

This work comprehends two distinct parts. Firstly, formulated zeolites with FAU topologies, specifically binderless zeolite NaY (Köstrolith® NAYBFK) and 13X (Köstrolith® 13XBFK) from Chemiewerk Bad Köstritz GmbH (CWK), and binder-containing 13X (SYLOBEAD® MS C 548, denoted by 13XB for simplicity) from Grace were compared through modeling and simulation for adsorption heating applications, using water as adsorbate. The necessary data for the AHPs simulations included: isosteric heats of adsorption ($Q_{\mathrm{ads}}$) assessed from experimental water adsorption isotherms; thermal conductivities ($\lambda_{\mathrm{eff,s}}$) of the adsorbents determined as function of temperature; measured solid densities ($\rho_{\mathrm{s}}$). The cyclic adsorption process was simulated accounting for a Box-Behnken design with four factors and three levels per factor: time of adsorption and desorption steps ($t_{\mathrm{ADS+DES}}$), temperature of condensation ($T_{\mathrm{cond}}$), temperature of the heat transfer fluid (HTF) in the desorption stage ($T_{\mathrm{HTF,hot}}$), and bed thickness ($\delta$). In the second part of this work, the statistical outcomes from DoE/RSM were analyzed, as: Pareto charts for assessing concomitant impact of operating/geometric parameters on *COP* and *SHP*, and polynomial equations for expeditious performance predictions as function of the factors (and *vice-versa*). Insights

into the usefulness of these outcomes for the optimization of AHEx designs and control strategies of AHPs are provided for NaYBFK, which was the best material found in terms of both *COP* and *SHP*.

## 2. Materials and methods

Zeolite NaY (Köstrolith® NaYBFK) was kindly provided by Chemiewerk Bad Köstritz GmbH (CWK), which also commercializes 13X (Köstrolith® 13XBFK). The material 13XB (SYLOBEAD® MS C 548) contains a mineral clay binder (inorganic), and was kindly provided by Grace.

The density ($\rho_s$) of NaYBFK and 13XB was measured by helium pycnometry using a Quantachrome Multipycnometer after pre-treatment of the powders at 473 K during 150 min (*ca.* 4 % error).

Pellets of NaYBFK and 13XB with 1 cm diameter and 0.5 cm thickness were prepared to measure the effective thermal conductivities ($\lambda_{eff,s}$) of the solid in the range 298.15–388.15 K, using the Gustafsson Probe method (or hot disk [48]) with a thermal constant analyzer TPS 2500S, and the samples temperature was controlled using a Thermo Scientific AC 200 immersion circulator. Prior to the data recording at a given temperature, the samples were maintained at constant temperature during 30 min. The accuracy of the measurements is *ca.* 5 %.

## 3. System description and mathematical modeling

### *3.1. Adsorbent Heat Exchanger (AHEx) geometry*

The simulations were performed for the AHEx unit schematically shown in Fig. 1. Amongst various designs reported in the literature [49], this simple geometry was chosen since it is representative for modeling and simulation, and well-studied in the literature [21, 35, 50], allowing to correctly evaluate trends and compare distinct adsorbent/adsorbate pairs.

*3.2. Modeling and performance indicators*

The mathematical model of the unsteady state AHEx unit was written for a differential volume element of radial thickness *dr*, and contemplates the material balance to the bed, the material balance to the adsorbent particle given by the Linear Driving Force (LDF) model, the energy balances to the adsorbent and vapour, the equilibrium isotherms, and the momentum balance given by Darcy's law. The corresponding equations, assumptions, initial and boundary conditions, and numerical approach are given in the Supplementary Information (Section 1). The adsorption isotherms for each working pair together with the linear driving force (LDF) model for mass transfer are given in Section 4.1.1 (Table 2, Eqs. (11)-(14)). The LDF model is an approximation to the material balance to the adsorbent particle, which, in its unapproximated form, embodies Fick's law [51]. Since it is simultaneously analytic, simple and physically consistent, the LDF model has been frequently and successfully used to describe gas and liquid adsorption kinetics [51-54]. Moreover, it has been successfully applied to describe intraparticle mass transfer kinetics in a fixed bed adsorption process with zeolite Köstrolith® 13XBFK (used in this work) [55].

For assessing the overall heating performance of each pair, the coefficient of performance and the specific heating power were calculated as follows:

$$COP = \frac{|Q_{\mathrm{ADS}} + Q_{\mathrm{cond}} + Q_{\mathrm{COOL}}|}{Q_{\mathrm{DES}} + Q_{\mathrm{HEAT}}} \quad (1)$$

$$SHP = \frac{|Q_{\mathrm{ADS}} + Q_{\mathrm{cond}} + Q_{\mathrm{COOL}}|}{m_{\mathrm{s}} t_{\mathrm{cycle}}} \quad (2)$$

where $Q_{\mathrm{ADS}}$, $Q_{\mathrm{COOL}}$ and $Q_{\mathrm{cond}}$ are, respectively, the heats released during isobaric adsorption, isosteric cooling and by the condenser, and $Q_{\mathrm{DES}}$ and $Q_{\mathrm{HEAT}}$ are the heats supplied to the bed during the isobaric desorption and isosteric heating stages, respectively; $m_{\mathrm{s}}$ is the mass of the adsorbent and $t_{\mathrm{cycle}}$ is the cycle time. The heats involved in the cycle were computed as follows:

$$Q_{\mathrm{ADS}} = \int_{T_{\mathrm{ADS,ini}}}^{T_{\mathrm{ADS,fin}}} \left[m_{\mathrm{s}}\left(C_{\mathrm{p,s}} + \bar{W} C_{\mathrm{p,a}}\right)\right] d\bar{T} + \int_{\bar{W}_{\mathrm{min}}}^{\bar{W}_{\mathrm{max}}} m_{\mathrm{s}}\,(-Q_{\mathrm{ads}}) d\bar{W} \quad (3)$$

$$Q_{\mathrm{HEAT}} = \int_{T_{\mathrm{HEAT,ini}}}^{T_{\mathrm{HEAT,fin}}} \left[m_{\mathrm{s}}\left(C_{\mathrm{p,s}} + \bar{W} C_{\mathrm{p,a}}\right)\right] d\bar{T} \quad (4)$$

$$Q_{\mathrm{DES}} = \int_{T_{\mathrm{DES,ini}}}^{T_{\mathrm{DES,fin}}} \left[m_{\mathrm{s}}\left(C_{\mathrm{p,s}} + \bar{W} C_{\mathrm{p,a}}\right)\right] d\bar{T} + \left| \int_{\bar{W}_{\mathrm{max}}}^{\bar{W}_{\mathrm{min}}} m_{\mathrm{s}}\, Q_{\mathrm{ads}} d\bar{W} \right| \quad (5)$$

$$Q_{\mathrm{COOL}} = \int_{T_{\mathrm{COOL,ini}}}^{T_{\mathrm{COOL,fin}}} \left[m_{\mathrm{s}}\left(C_{\mathrm{p,s}} + \bar{W} C_{\mathrm{p,a}}\right)\right] d\bar{T} \quad (6)$$

$$Q_{\mathrm{cond}} = -m_{\mathrm{s}} \Delta\bar{W}_{\mathrm{cycle}} \Delta H_{\mathrm{v}}\ , \quad \text{where } \Delta\bar{W}_{\mathrm{cycle}} = \bar{W}_{\mathrm{max}} - \bar{W}_{\mathrm{min}} \quad (7)$$

where $C_{\mathrm{p,s}}$ and $C_{\mathrm{p,a}}$ are, respectively, the specific heat capacities of the adsorbent and adsorbate, $Q_{\mathrm{ads}}$ is the isosteric heat of adsorption, $\Delta\bar{W}_{\mathrm{cycle}}$ is the cyclic average loading and $\Delta H_{\mathrm{v}}$ is the latent heat of vaporization of the refrigerant. The mass of the metal components of the AHEx was not considered in Eqs. (3)-(6), in order to extract specific information regarding the influence of distinct adsorbents. The metal contribution hinders *COP*, albeit the major *COP* trends may be similar with or without this contribution [56, 57].

The average temperature ($\bar{T}$), pressure ($\bar{P}$) and loading ($\bar{W}$) in the bed along time (generically denoted by $\bar{\varphi}$) were given by:

$$\bar{\varphi}(t) = \frac{\int_{R_\mathrm{i}}^{R_\mathrm{o}} 2r\varphi(t,r)dr}{(R_\mathrm{o}^2 - R_\mathrm{i}^2)} \tag{8}$$

where $t$ denotes time, $r$ is the spatial coordinate, and $R_\mathrm{o}$ and $R_\mathrm{i}$ are, respectivelly, the external and internal boundaries of the adsorbent bed (Fig. 1).

*3.3. Design of experiments and response surface methodology (DoE/RSM)*

DoE/RSM consists of a set of mathematical and statistical methods which fit empirical models to experimental data (or simulation results). For applying this technique, it is necessary to specify the factors (independent variables), the responses (dependent variables), the levels of the factors (degrees of variation), the experimental domain (minimum and maximum limits of the factors) and the experimental design method [58]. In this work, a Box-Behnken design was adopted, which is efficient and economical, requiring a number of simulations given by $N = 2k(k-1) + cp$, where $cp$ is the number of central points and $k$ is the number of factors, and is adequate when data may present curvatures [58]. Due to the importance of both operating conditions and geometric parameters in the performance of AHPs, the statistical studies considered the time of the adsorption and desorption stages ($t_{\mathrm{ADS+DES}}$), the condensation and heat source temperatures ($T_{\mathrm{cond}}$ and $T_{\mathrm{HTF,hot}}$, respectively), and the bed thickness ($\delta$), with three levels per factor, as summarized in Table 1. The values of the independent variables were codified according to Eq. (9), for ranging between -1 and 1:

$$X_\mathrm{k} = \frac{x_\mathrm{k} - x_0}{\Delta x_\mathrm{k}} \tag{9}$$

where $X_k$ and $x_k$ are, respectively, the codified and real values of the independent variable, $x_0$ is its real value at the central point, and $\Delta x_k$ is its step change. The $T_{cond}$ is between 308.15 and 328.15 K, which allows the utilization of the heat produced by the AHP for hot water production, while $T_{HTF,hot}$ ranges from 398.15 K (which enables the use of water as HTF) to 448.15 K (that implies alternative HTFs such as thermal oils, due to pressure constraints in circuits).

The results submitted to the RSM analysis are usually well represented by a second order polynomial. In the case of our simulations, the same equations are adopted:

$$Y = \beta_0 + \sum_{i=1}^{k} \beta_i X_i + \sum_{i=1}^{k} \beta_{ii} X_i^2 + \sum_{1 \le i < j}^{k} \beta_{ij} X_i X_j \quad (10)$$

where $Y$ is the response (*COP* or *SHP*), $X_i$ and $X_j$ are the codified factors ($t_{ADS+DES}$, $T_{cond}$, $T_{HTF,hot}$, $\delta$), $\beta_0$ is a constant including the residual, and $\beta_i$, $\beta_{ii}$ and $\beta_{ij}$ are model coefficients related to linear, quadratic and pair interaction effects, respectively.

STATISTICA software (version 5.1, StatSoft Inc., Tulsa, USA) was used for statistical modeling and treatment of the simulation results. An analysis of variance (ANOVA) was performed to assess the statistical significance of factors and interactions using Fisher's test and its associated probability level (*p*-value) for a confidence interval of 95 %. For judging the significance of the estimated coefficients $\beta_i$, $\beta_{ii}$, $\beta_{ij}$, *t*-tests were performed. The coefficient of determination ($R^2$) and its adjusted value ($R^2_{adj}$) were used to evaluate the goodness of fit of the regression models.

## 4. Results and discussion

### *4.1. Measurement and determination of properties of NaYBFK and 13XB*

The Dubinin-Astakhov model was fitted to equilibrium data of water vapour onto zeolites NaYBFK and 13XB, from which heats of adsorption were calculated, and the solid densities and temperature dependency of thermal conductivities were measured. Morphological and textural data (SEM images, $N_2$ isotherms, and specific surface area and pore volume) for NaYBFK and 13XB are given in the Supplementary Information (Section 2.1), and for 13XBFK are reported in Schumann *et al.* [59]. The properties necessary for the simulations using the latter adsorbent were collected from Mette *et al.* [55].

*4.1.1. Water vapour isotherms, heats of adsorption and adsorption kinetics*

For 13XBFK, the water adsorption isotherm in the temperature range 298.15 – 523.15 K was taken from literature [55] (Eq. (11), Table 2). In the case of the other two adsorbents, the Dubinin-Astakhov (DA) model, often used to describe the adsorption equilibrium in zeolites and zeotypes [2, 55, 60], was accurately fitted to data provided by Chemiewerk Bad Köstritz GmbH (CWK) for NaYBFK in the range 298.15 – 353.15 K (Fig. 2), and to data from Grace for 13XB in the range 298.15 – 423.15 K (Fig. 3). For NaYBFK, the parameters of the model obtained by unconstrained nonlinear optimization are: $W_0 = 0.301$ kg kg$^{-1}$, $C = 2.62\times10^{-8}$ K$^{-2.33}$ and $n = 2.33$ (see Eq. (12), Table 2), with an average absolute relative deviation (AARD) of 3.5 %. In the case of 13XB, they are: $W_0$ = 0.231 kg kg$^{-1}$, $C$ = $6.28\times10^{-9}$ K$^{-2.41}$ and $n = 2.41$ (see Eq. (13), Table 2), with AARD = 6.2 %.

The isosteric heats of adsorption ($Q_{\mathrm{ads}}$) at half coverage for NaYBFK and 13XB were determined using the isotherm model and the Clausius-Clapeyron equation (Supplementary Information, Section 2.2), and are equal to $3.05\times10^{6}$ J kg$^{-1}$ and

$3.34\times10^6$ J $kg^{-1}$, respectively, which are in close agreement (less than 10 % differences) with literature data [62, 63]. For 13XBFK, $Q_{ads}$ = $3.50\times10^6$ J $kg^{-1}$ is reported by Mette *et al.* [55].

Regarding kinetics, an estimation of the mass transfer resistances inside the porous structure highlighted greater resistances in macropores and mesopores than in micropores (detailed in the Supplementary Information, Section 2). Hence, Eq. (14) (Table 2) is appropriate for calculating $K_{LDF}$ [51].

*4.1.2. Solid densities ($\rho_s$) and thermal conductivities ($\lambda_{eff,s}$)*

The measured values of $\rho_s$ for NaYBFK and 13XB are 2475 and 2447 kg $m^{-3}$, respectively (Table 3), which are in agreement with literature data for zeolites [65] (details in the Supplementary Information, Section 2).

Fig. 4 shows $\lambda_{eff,s}$ of NaYBFK ($\lambda_{eff,NaYBFK}$) and 13XB ($\lambda_{eff,13XB}$) measured as function of temperature in the range 298.15-388.15 K, and corresponding linear fittings (details in the Supplementary Information, Section 2). In the simulations, average values of $\lambda_{eff,s}$ between the minimum and the maximum temperatures of the bed were used, which are in the range 0.272 – 0.293 W $m^{-1}$ $K^{-1}$ and 0.272 – 0.281 W $m^{-1}$ $K^{-1}$ for NaYBFK and 13XB, respectively (Table 3). These results are in agreement with literature data for zeolites, generally in the range 0.2-0.4 W $m^{-1}$ $K^{-1}$ [66, 67].

*4.2. Simulation studies and optimization through DoE/RSM*

In the first part of this section, the performances of NaYBFK, 13XBFK and 13XB for adsorption heating applications are investigated by carrying out a set of simulations,

defined according to a Box-Behnken design with four factors ($t_{\mathrm{ADS+DES}}$, $T_{\mathrm{cond}}$, $T_{\mathrm{HTF,hot}}$ and $\delta$) and three levels (Table 1). The main properties of the adsorbent/adsorbate pairs considered in the simulations are given in Table 3. In the second part, the statistical outcomes from DoE/RSM obtained for NaYBFK are presented and discussed, which include: Pareto charts showing the ranking of effects on *COP* and *SHP*; polynomial equations from RSM for predicting the AHP performance as function of the factors (and *vice-versa*). Examples of the usefulness of these equations to map the system performance and to easily select optimal operation times and geometric AHEx parameters are presented.

*4.2.1. Comparison of NaYBKF, 13XBFK and 13XB beds*

Table 4 shows the set of simulations run for the conditions established by the Box-Behnken design of four factors ($t_{\mathrm{ADS+DES}}$, $T_{\mathrm{cond}}$, $T_{\mathrm{HTF,hot}}$ and $\delta$) and three levels listed in Table 1, along with the results of *COP* and *SHP* obtained for NaYBFK, 13XBFK and 13XB. The material NaYBFK seems to lead to superior AHP performances than 13XBFK and 13XB, which is closely related to the higher values of $\Delta\bar{W}_{\mathrm{cycle}}$ within the range of operating conditions under study. The two latter materials led to roughly comparable results, suggesting that the presence of the clay binder in 13XB does not affect considerably its performance. Based on these results, the formulation used to produce commercial 13XB seems very efficient, avoiding loss of material performance.

*4.2.2. Statistical outcomes from DoE/RSM for NaYBKF and insights into AHPs optimization*

*4.2.2.1. Impact of operating/geometric factors on COP and SHP*

Pareto charts allow the identification and classification of the factors and interactions with (negative or positive) impact on a response variable.

Fig. 5 shows the Pareto charts of *COP* and *SHP* for the Box-Behnken design matrix of Table 4, with confidence interval of 95 %, where factors with positive and negative effects are ranked.

The increase of $T_{\mathrm{cond}}$ has negative influence on the performance parameters, being the greatest impacting variable on *COP* (Fig. 5(a)). As $T_{\mathrm{cond}}$ increases, the pressure during desorption stage increases, leading to the decrease of the average loading swing ($\Delta\bar{W}_{\mathrm{cycle}}$) and of the heats generated per cycle. The bed thickness ($\delta$) is the second most important factor on *COP*, and its increase predominantly reduces *SHP*. Incrementing $\delta$ increases the resistance to heat transfer along the adsorbent bed, influencing the heating/cooling rates of the adsorbent, and ultimately the adsorption/desorption rates of water vapour. Higher $T_{\mathrm{HTF,hot}}$ impacts favorably on the AHEx operation, since it allows better adsorbent regeneration and thus higher $\Delta\bar{W}_{\mathrm{cycle}}$. The $t_{\mathrm{ADS+DES}}$ (ranked in fourth place in both Pareto charts) influences *COP* positively, since more time is given to heat and mass transfer, approximating the system to equilibrium state, which enlarges the differences between adsorption and desorption steps ($\Delta\bar{W}_{\mathrm{cycle}}$). However, higher $t_{\mathrm{ADS+DES}}$ accounts for reduced *SHP*. There are quadratic ($t_{\mathrm{ADS+DES}}^2$, $\delta^2$) and interaction effects ($T_{\mathrm{cond}} \times T_{\mathrm{HTF,hot}}$, $\delta \times t_{\mathrm{ADS+DES}}$) with statistical significance for *COP* and *SHP*, albeit less important. The Pareto charts for 13XBFK and 13XB present similar trends to those for NaYBFK (Supplementary Information, Section 3). Overall, these results show that DoE/RSM can be successfully applied for the evaluation of impact of operating conditions and geometric parameters on the performance of AHPs.

*4.2.2.2. RSM models for COP and SHP*

The RSM results of *COP* and *SHP*, for which $R^2_{COP} = 0.981, R^2_{\text{adj},COP} = 0.973$, $R^2_{SHP} = 0.978$ and $R^2_{\text{adj},SHP} = 0.967$, are:

$$COP = 29.905 + 6.686 \times 10^{-5} t_{\text{ADS+DES}} - 9.390 \times 10^{-2} T_{\text{cond}} - 5.692 \times 10^{-2} T_{\text{HTF,hot}} - 54.667\delta - 1.403 \times 10^{-8} t^2_{\text{ADS+DES}} + 8.148 \times 10^{-3} t_{\text{ADS+DES}}\delta + 1.900 \times 10^{-4}\, T_{\text{cond}} T_{\text{HTF,hot}} \quad (15)$$

$$SHP = 3015.673 - 1.199 \times 10^{-1} t_{\text{ADS+DES}} - 17.250 T_{\text{cond}} + 8.163 T_{\text{HTF,hot}} - 295411\delta + +4044096\delta^2 + 11.259 t_{\text{ADS+DES}}\delta + 1400 T_{\text{cond}}\delta - 652 T_{\text{HTF,hot}}\delta \quad (16)$$

These simple equations are very useful for expeditious performance predictions since considerable number of experiments or time consuming simulations are avoided, for example, when a significant number of grid points need to be used to eliminate numerical instabilities due to the non-linearity and stiffness of the equations, or even when the isotherms are described by non-linear algebraic expressions (which greatly prolongs the simulation time). Examples of the usefulness of these equations are presented in the following.

*(i) Mapping the AHP performance and assessing trends*

The Eqs. (15)-(16) enable mapping the system performance within a range of conditions, based on the small number of simulations accomplished above. This may be visualized using e.g. surface plots, which show the shape of the response surfaces, and allow assessing trends and identifying minima and maxima when existent. As illustrative case, the surface plots of *COP* and *SHP* as function of $T_{\text{HTF,hot}}$ and $\delta$, with fixed $T_{\text{cond}}$ = 318.15 K and $t_{\text{ADS+DES}}$ = 2250 s, are given in Fig. 6. As side remark, maximum values of *COP* and *SHP* around 1.50 and 400 W kg$^{-1}$, respectively, are achievable for $T_{\text{HTF,hot}}$ = 448.15 K and $\delta = 5\times10^{-3}$ m, which indicates somewhat

limited performances (namely in terms of power) for NaYBFK. Besides, $T_{\mathrm{HTF,hot}}$ = 448.15 K mimics a practical scenario requiring the use of thermal oils or even exhaust gases for bed regeneration. This may turn the concept of the AHP unfeasible in some applications, due to technical complexity, maintenance efforts (e.g. need for periodical oil replacement) and costs. Regarding $\delta$, the results reiterate the need for developing coated AHExs, for example using dip coating or spray coating techniques, for which $\delta$ <1 mm is commonly found [70], or even through the synthesis of thin adsorbent coatings (with dozens or hundreds of microns) directly on the heat exchangers [70, 71], in order to increase the technical and economic viability of AHPs (albeit a good compromise in terms of metal to adsorbent mass ratio is necessary to not significantly hinder *COPs*). Coated AHExs enable *SHPs* > 1000 W kg$^{-1}$, while loose grains or pellets generally do not exceed the order of hundreds: e.g., Dawoud [5], Restuccia and Cacciola [21] and Dawoud et al. [23] report *SHP* values in the range of *ca.* 900 – 2200 W kg$^{-1}$ for coatings of zeolites/zeotypes, while for beds of loose pellets they were roughly in the interval 160 – 550 W kg$^{-1}$. The latter range of *SHPs* is somewhat in agreement with the values in Figs. 6-7 in the interval *ca.* 100 - 600 W kg$^{-1}$.

*(ii) Optimum times to fullfil performance requirements - insights into AHP control strategies*

In this section, the selection of optimum times to meet specific performance requisites under variable $T_{\mathrm{cond}}$ is exemplified, envisaging two distinct control strategies, in which either *SHP* or *COP* are to be maximized. Fig. 7(a)-(b) shows the contour plots of *COP* and *SHP* (Eqs. (15)-(16)) as function of $T_{\mathrm{cond}}$ and $t_{\mathrm{ADS+DES}}$, under fixed $T_{\mathrm{HTF,hot}} = 448.15$ K and $\delta = 5\mathrm{x}10^{-3}$ m, from which optimum times of operation can be

extracted. In the following discussion it is always assumed that $T_{\mathrm{cond}}$ should range from 308.15 to 328.15 K in order to meet consumer needs (this mimics the domestic hot water production, in which the water temperature inside the tank rises along time).

*Control strategy for maximizing SHP*. If along the heating process $COP \geq 1.40$ and the highest *SHP* are simultaneously required, the evolution of $(t_{\mathrm{ADS+DES}}, T_{\mathrm{cond}})$ pair can be easily designed as shown in Fig. 7(a) (filled circles). In the first 3 cycles ($308.15 \leq T_{\mathrm{cond}}(\mathrm{K}) \leq 318.15$), an optimum $t_{\mathrm{ADS+DES}}$ of 900 s is identified, and a progressive decrease in the performance occurs (*COP*: 1.51 > 1.47 > 1.42; calculated from Eq. (15)), for which the corresponding *SHPs* ($\mathrm{W\,kg^{-1}}$) in Fig. 7(b) are: 621 > 570> 519; calculated from Eq. (16). In the fourth and fifth cycles ($T_{\mathrm{cond}} = 323.15$ and 328.15 K, respectively), $t_{\mathrm{ADS+DES}}$ needs to be increased to *ca.* 1260 s and 1800 s, in order to meet *COP* = 1.40 and maximum *SHP* values around 450 and 360 $\mathrm{W\,kg^{-1}}$ (Fig. 7(b)), respectively.

*Control strategy for maximizing COP*. Fixing $SHP \geq 400\ \mathrm{W\,kg^{-1}}$ and seeking for the highest *COP* values at each moment during the heating process, the resulting evolution of $t_{\mathrm{ADS+DES}}$ can be easily established from Fig. 7(b) (open white circles). In the first and second heating cycles ($T_{\mathrm{cond}}$ of 308.15 K and 313.15 K, respectively), $t_{\mathrm{ADS+DES}} = 3600$ s allows $SHP \geq 400\ \mathrm{W\,kg^{-1}}$ and maximizes *COP* (which attains, respectively, 1.63 and 1.59 (Fig. 7(a)). From the second to the third cycle, $t_{\mathrm{ADS+DES}}$ needs to be reduced from 3600 to *ca.* 2700 s, while in the fourth cycle ($T_{\mathrm{cond}} = 323.15$ K) it must be further decreased to *ca.* 1980 s. The heating process ends in the fifth cycle ($T_{\mathrm{cond}} = 328.15$ K), for which $t_{\mathrm{ADS+DES}}$ rounds 1170 s, *SHP* is *ca.* 400 $\mathrm{W\,kg^{-1}}$ and *COP* approaches 1.36 (Fig. 7(a)).

Overall, DoE/RSM methodologies may aid the development of advanced AHP control strategies allowing adaptions to changes in working conditions and/or user requirements, while simultaneously meeting performance requisites.

*(iii) Optimal ($\delta$,$t_{\mathrm{ADS+DES}}$) pairs to meet performance requirements - insights into the development of optimized AHExs*

Fig. 8(a)-(c) shows (*SHP*, *COP*) pairs estimated using Eqs. (15)-(16) for $T_{\mathrm{HTF,hot}} =$ 448.15 K, $\delta$ and $t_{\mathrm{ADS+DES}}$ in the range $5 \times 10^{-3} - 10\times 10^{-3}$ m and 900 – 3600 s, respectively, and $T_{\mathrm{cond}}$ of 308.15 K, 318.15 K and 328.15 K. Exemplified requisites of *COP* ≥ 1.40 and *SHP* ≥ 400 W kg$^{-1}$ are marked. The $\delta$ *vs.* $t_{\mathrm{ADS+DES}}$ values considered in the performance estimations for each $T_{\mathrm{cond}}$ are also shown, where the combinations that satisfy *COP* and *SHP* requisites are highlighted with orange border.

For $T_{\mathrm{cond}}$ = 308.15 K (Fig. 8(a)), the performance requisites are met for $\delta = 5 \times 10^{-3}$ m in a broad range of $t_{\mathrm{ADS+DES}}$ (900 – 3600 s), and for $\delta = 6.25 \times 10^{-3}$ m with $t_{\mathrm{ADS+DES}}$ lower than ~ 2750 s. Incrementing $T_{\mathrm{cond}}$ to 318.15 K (Fig. 8(b)), only $\delta = 5 \times 10^{-3}$ m with $t_{\mathrm{ADS+DES}}$ < 2750 s allows fulfilling the *COP* and *SHP* requirements. For $T_{\mathrm{cond}}$ = 328.15 K (Fig. 8(c)), the pre-established performance requisites are no longer met for any evaluated ($\delta$, $t_{\mathrm{ADS+DES}}$) pairs evaluated. This example shows the importance of analyzing the complete range of temperature conditions when seeking for optimal AHEx geometry and operating parameters.

In the whole, DoE/RSM can easily aid the identification of optimal combinations of operating and geometric features for meeting pre-established performance requisites.

## Conclusions

Modeling and simulation studies were accomplished to compare the performance of binderless NaY (NaYBFK), binderless 13X (13XBFK), and binder-containing 13X (13XB) for adsorption heating applications using water as refrigerant. Equilibrium, kinetic and thermophysical properties were measured and/or estimated to carry out 25 simulations per adsorbent totally. With this purpose, four factors and three levels were studied according to a Box-Behnken design: $t_{\mathrm{ADS+DES}}$ between 900 and 3600 s; $T_{\mathrm{cond}}$ from 308.15 to 328.15 K; $T_{\mathrm{HTF,hot}}$ from 398.15 to 448.15 K; and $\delta$ between $5\times10^{-3}$ and $10\times10^{-3}$ m. The NaYBFK was the most promising adsorbent, with *COP* values up to 1.63 and *SHP* around 620 W $\mathrm{kg}^{-1}$. The 13XBFK and 13XB materials achieved similar *COP* and *SHP* results, which means that the mineral clay binder of 13XB does not hinder its performance within the studied range of conditions.

In a second part of the work, the statistical outcomes from DoE/RSM for NaYBFK beds were analyzed, and insights into their usefulness for the optimization of adsorption heating pumps (AHPs) were illustrated. Simple models for the quick estimation of *COP* and *SHP* were developed, allowing for: (i) mapping system performance in a broad range of conditions with small number of simulations; (ii) the selection of optimal operating times and geometric features of adsorption heat exchangers (AHExs) under pre-established performance requirements. Overall, DoE/RSM can aid the successful development of optimized AHExs and advanced AHP control strategies.

**Acknowledgements**

This work was developed in the scope of the project CICECO-Aveiro Institute of Materials (Ref. FCT UID/CTM/50011/2013), financed by national funds through the FCT/MEC and when applicable co-financed by FEDER under the PT2020 Partnership Agreement. The authors are grateful to Doctoral Program EngIQ, Fundação para a Ciência e Tecnologia (FCT) and Bosch Thermotechnology for a PhD grant (PD/BDE/113538/2015) to Joana M. Pinheiro. The authors thank Chemiewerk Bad Köstritz GmbH (CWK) for providing the binderless NaY material (Köstrolith® NaYBFK), and for the authorization to use the respective water adsorption isotherms data. Grace is acknowledged for providing the material SYLOBEAD® MS C 548 (13XB). The authors thank Professor Vítor Amaral (CICECO, UA) for the measurements of the thermal conductivities of zeolites (supported through the project "Facing the challenges of characterizing novel thermal materials and processes (Heat@UA)", RECI/CTM-CER/0336/2012 co-financed by FEDER, QREN reference COMPETE: FCOMP-01-0124-FEDER-027465).

**Nomenclature**

| | |
|---|---|
| AARD | $= \frac{\sum_{i=1}^{n} \left\lvert \frac{Value_{calculated,i} - Value_{experimental,i}}{Value_{experimental,i}} \right\rvert}{Ndata}$ |
| | Average Absolute Relative Deviation (%) |
| $cp$ | Number of central points in Box-Behnken design |
| $C$ | Parameter of Dubinin-Astakhov isotherm |
| $C_{\mathrm{p}}$ | Specific heat capacity (J kg$^{-1}$ K$^{-1}$) |
| $COP$ | Coefficient of performance |
| $d_{\mathrm{p}}$ | Adsorbent particle diameter (m) |
| $D_{\mathrm{eff}}$ | Effective diffusivity (m$^2$ s$^{-1}$) |
| $D_{\mathrm{K}}$ | Knudsen diffusivity (m$^2$ s$^{-1}$) |
| $D_{\mathrm{m}}$ | Molecular diffusivity (m$^2$ s$^{-1}$) |
| $H$ | Equilibrium constant |
| $k$ | Number of factors in the Box-Behnken design |
| $K_{\mathrm{LDF}}$ | Linear driving force (LDF) global mass transfer coefficient (s$^{-1}$) |
| $m$ | Mass (kg) |
| $M$ | Molar mass of adsorbate (kg mol$^{-1}$) |
| $n$ | Parameter of Dubinin-Astakhov isotherm |
| $N$ | Number of runs in Box-Behnken design |
| $P$ | Pressure (Pa) |
| $Q$ | Heat (J) |
| $Q_{\mathrm{ads}}$ | Isosteric heat of adsorption (J kg$^{-1}$) |

| | |
|---|---|
| $Q_{\mathrm{ADS}}$ | Heat released during the isobaric adsorption stage (J), |
| $Q_{\mathrm{COOL}}$ | Heat released during the isosteric cooling stage (J) |
| $Q_{\mathrm{cond}}$ | Heat released by the condenser (J) |
| $Q_{\mathrm{DES}}$ | Heat supplied during the isobaric desorption stage (J) |
| $Q_{\mathrm{HEAT}}$ | Heat supplied during the isosteric heating stage (J) |
| $r$ | Spatial coordinate (m) |
| $R$ | Radial position in the adsorbent bed (m) |
| $\Re$ | Universal gas constant (J mol$^{-1}$ K$^{-1}$). |
| $R^2$ | Coefficient of determination |
| $R^2_{\mathrm{adj}}$ | Adjusted coefficient of determination |
| $R_{\mathrm{p}}$ | Adsorbent particle radius (m) |
| $SHP$ | Specific heating power (W kg$^{-1}$) |
| $t$ | Time (s) |
| $t_{\mathrm{cycle}}$ | Cycle time (s) |
| $T$ | Temperature (K) |
| $T_{\mathrm{HTF,cool}}$ | Temperature of the cool heat transfer fluid (K) |
| $T_{\mathrm{HTF,hot}}$ | Temperature of the hot heat transfer fluid (K) |
| $W$ | Adsorbate loading (kg kg$^{-1}$) |
| $W_0$ | Adsorbate loading at saturation pressure (kg kg$^{-1}$) |
| $x_0$ | Real value of the factor at the central point in DoE/RSM analysis |
| $x_{\mathrm{k}}$ | Real value of the factor in DoE/RSM analysis |

| | |
|---|---|
| $X_k$, $X_i$, $X_j$ | Codified value of the factor in DoE/RSM analysis |
| $Y$ | Response variable in DoE/RSM analysis |

*Greek symbols*

| | |
|---|---|
| $\beta_0$ | RSM model constant including the residual |
| $\beta_i$ | RSM model coefficient related to linear effects |
| $\beta_{ii}$ | RSM model coefficient related to quadratic effects |
| $\beta_{ij}$ | RSM model coefficient related to pair interaction effects |
| $\beta_{water}$ | Thermal expansion coefficient of water ($K^{-1}$) |
| $\delta$ | Adsorbent bed thickness (m) |
| $\Delta H_v$ | Latent heat of vaporization (J $kg^{-1}$) |
| $\Delta \bar{W}_{cycle}$ | Cyclic average adsorption loading swing (kg $kg^{-1}$) |
| $\Delta x_k$ | Step change of the real value of the factor in DoE/RSM analysis |
| $\varepsilon_b$ | Porosity of the bed |
| $\varepsilon_p$ | Porosity of the particle |
| $\lambda$ | Thermal conductivity (W $m^{-1}$ $K^{-1}$) |
| $\Omega$ | LDF model constant dependent on the particle geometry |
| $\rho$ | Density (kg $m^{-3}$) |
| $\tau_p$ | Tortuosity of the particle |
| $\varphi$ | Generic notation of $T$, $W$ and $P$ |
| $\bar{\varphi}$ | Generic notation of $\bar{T}$ , $\bar{W}$ and $\bar{P}$ |

*Subscripts*

| | |
|---|---|
| a | Adsorbate |
| ADS | Isobaric adsorption stage |
| cond | Condenser |
| COOL | Isosteric cooling stage |
| DES | Isobaric desorption stage |
| eff | Effective |
| eq | Equilibrium |
| evap | Evaporator |
| fin | Final |
| HEAT | Isosteric heating stage |
| i | Internal boundary of the bed |
| ini | Initial |
| max | Maximum |
| min | Minimum |
| o | External boundary of the bed |
| p | Particle |
| s | Adsorbent |
| sat | Saturation |

**Figure captions**

Figure 1 - Schematic representation of the cylindrical adsorbent heat exchanger (AHEx) studied in this work.

Figure 2 - Adsorption isotherms of water vapour on zeolite NaYBFK: experimental data at 298.15 (o), 333.15 (◊) and 353.15 K (□) provided by Chemiewerk Bad Köstritz GmbH (CWK); lines are the Dubinin-Astakhov model fitting.

Figure 3 - Adsorption isotherms of water vapour on zeolite 13XB: experimental data at 298.15 (o), 313.15 (◊), 338.15 K (Δ), 368.15 K (□) and 423.15 K (▽) provided by Grace [61]; lines are the Dubinin-Astakhov model fitting.

Figure 4 - Variation of $\boldsymbol{\lambda_{eff,s}}$ of 13XB and NaYBFK with temperature. Squares are experimental results (using the Gustafsson probe method), and lines are the corresponding linear fittings.

Figure 5 - Pareto charts of (a) *COP* and (b) *SHP* for NaYBFK considering the Box-Behnken design of Table 4 with confidence interval of 95 %.

Figure 6 - Surface plots of (a) *COP* (Eq. (15)) and (b) *SHP* (Eq. (16)) as function of $\boldsymbol{T_{HTF,hot}}$ and $\boldsymbol{\delta}$ obtained for NaYBFK with $\boldsymbol{T_{cond}}$ = 318.15 K and $\boldsymbol{t_{ADS+DES}}$ = 2250 s. Dots are simulation results (Table 4, runs 13 and 18-21).

Figure 7 - Contour plots of (a) *COP* (Eq.(15)) and (b) *SHP* (Eq. (16)) obtained for NaYBFK as function of $\boldsymbol{T_{cond}}$ and $\boldsymbol{t_{ADS+DES}}$, for fixed $\boldsymbol{T_{HTF,hot}} = 448.15$ K and $\boldsymbol{\delta} =$ 5x10$^{-3}$ m. Filled black circles to the specification requiring $COP \geq 1.40$ and the simultaneous maximization of *SHP* in all cycles; Open white circles concern the requisite of $SHP \geq 400$ $\mathbf{W\,kg^{-1}}$ and the concomitant maximization of *COP* in all cycles.

Figure 8 – Pairs of *SHP* and *COP* estimated using Eqs. (15)-(16) for $\boldsymbol{T_{HTF,hot}} = 448.15$ K, $\boldsymbol{\delta}$ and $\boldsymbol{t_{ADS+DES}}$ in the range $5 \times \mathbf{10^{-3}} -$ $10 \times \mathbf{10^{-3}}$ m and 900 – 3600 s, respectively, and $\boldsymbol{T_{cond}}$ of (a) 308.15 K, (b) 318.15 K and (c) 328.15 K. Exemplified performance requisites of $COP \geq 1.40$ and $SHP \geq 400$ W kg$^{-1}$ are marked (orange squares). The ($\boldsymbol{\delta}$, $\boldsymbol{t_{ADS+DES}}$) pairs considered for the performance estimations at each $\boldsymbol{T_{cond}}$ are also shown (black circles), where the combinations that allow meeting the *COP* and *SHP* requisites are highlighted (diamonds with orange border).

## References

[1] B.O. Bolaji, Z. Huan, Ozone depletion and global warming: Case for the use of natural refrigerant – a review, Renewable and Sustainable Energy Reviews, 18 (2013) 49-54.
[2] J.M. Pinheiro, S. Salústio, J. Rocha, A.A. Valente, C.M. Silva, Analysis of equilibrium and kinetic parameters of water adsorption heating systems for different porous metal/metalloid oxide adsorbents, Applied Thermal Engineering, 100 (2016) 215-226.
[3] D. Ürge-Vorsatz, L.F. Cabeza, S. Serrano, C. Barreneche, K. Petrichenko, Heating and cooling energy trends and drivers in buildings, Renewable and Sustainable Energy Reviews, 41 (2015) 85-98.
[4] F. Meunier, Adsorption heat powered heat pumps, Applied Thermal Engineering, 61 (2013) 830-836.
[5] B. Dawoud, On the development of an innovative gas-fired heating appliance based on a zeolite-water adsorption heat pump; system description and seasonal gas utilization efficiency, Applied Thermal Engineering, 72 (2014) 323-330.
[6] J.M. Pinheiro, A.A. Valente, S. Salústio, N. Ferreira, J. Rocha, C.M. Silva, Application of the novel ETS-10/water pair in cyclic adsorption heating processes: Measurement of equilibrium and kinetics properties and simulation studies, Applied Thermal Engineering, 87 (2015) 412-423.
[7] J.K. Kiplagat, R.Z. Wang, R.G. Oliveira, T.X. Li, M. Liang, Experimental study on the effects of the operation conditions on the performance of a chemisorption air conditioner powered by low grade heat, Applied Energy, 103 (2013) 571-580.
[8] G. Restuccia, A. Freni, G. Maggio, A zeolite-coated bed for air conditioning adsorption systems: parametric study of heat and mass transfer by dynamic simulation, Applied Thermal Engineering, 22 (2002) 619-630.
[9] H. Demir, M. Mobedi, S. Ülkü, A review on adsorption heat pump: Problems and solutions, Renewable and Sustainable Energy Reviews, 12 (2008) 2381-2403.
[10] D.B. Boman, D.C. Hoysall, D.G. Pahinkar, M.J. Ponkala, S. Garimella, Screening of working pairs for adsorption heat pumps based on thermodynamic and transport characteristics, Applied Thermal Engineering, 123 (2017) 422-434.
[11] A. Frazzica, A. Freni, Adsorbent working pairs for solar thermal energy storage in buildings, Renewable Energy, 110 (2017) 87-94.
[12] A. Freni, G. Maggio, A. Sapienza, A. Frazzica, G. Restuccia, S. Vasta, Comparative analysis of promising adsorbent/adsorbate pairs for adsorptive heat pumping, air conditioning and refrigeration, Applied Thermal Engineering, 104 (2016) 85-95.
[13] S.K. Henninger, S.-J. Ernst, L. Gordeeva, P. Bendix, D. Fröhlich, A.D. Grekova, L. Bonaccorsi, Y. Aristov, J. Jaenchen, New materials for adsorption heat transformation and storage, Renewable Energy, 110 (2017) 59-68.
[14] Chemiewerk Bad Köstritz GmbH (CWK) Products, Köstrolith zeolite molecular sieves. http://www.cwk-bk.de/en/produkte/molekularsiebe/zeolithe/, 2017 (accessed 20.01.2017).
[15] B. Alfons, K. Schumann, U. Baldur, Bindemittelfreies zeolithisches Granulat mit Faujasitstruktur und Verfahren zur Herstellung eines derartigen bindemittelfreien zeolithischen Granulats nebst Verwendung, DE102012010109 A1, Chemiewerk Bad Köstritz GmbH (2012).
[16] J. Jänchen, K. Schumann, E. Thrun, A. Brandt, B. Unger, U. Hellwig, Preparation, hydrothermal stability and thermal adsorption storage properties of binderless zeolite beads, International Journal of Low-Carbon Technologies, 7 (2012) 275-279.
[17] B. Jha, D.N. Singh, Basics of Zeolites, in: Fly Ash Zeolites: Innovations, Applications, and Directions, Springer Singapore, Singapore, 2016, pp. 5-31.
[18] P. Bendix, G. Füldner, M. Möllers, H. Kummer, L. Schnabel, S. Henninger, H.-M. Henning, Optimization of power density and metal-to-adsorbent weight ratio in coated adsorbers for adsorptive heat transformation applications, Applied Thermal Engineering, 124 (2017) 83-90.

[19] J.M. Corberan, M. Axell, R.d. Boer, A. Freni, U. Jakob, S. Landolina, P. Lundqvist, M. Monsberger, R. Nordman, T. Nowak, T. Oltersdorf, S. Spoelstra, F. Ziegler, Heat Pumps, in: Strategic Research Priorities for Cross-cutting Technology, Global CCS Institute, European Technology Platform on Renewable Heating and Cooling, Belgium, 2012, pp. 48-75.
[20] Y.B. Gui, R.Z. Wang, W. Wang, J.Y. Wu, Y.X. Xu, Performance modeling and testing on a heat-regenerative adsorptive reversible heat pump, Applied Thermal Engineering, 22 (2002) 309-320.
[21] G. Restuccia, G. Cacciola, Performances of adsorption systems for ambient heating and air conditioning, International Journal of Refrigeration, 22 (1999) 18-26.
[22] A. Sapienza, S. Santamaria, A. Frazzica, A. Freni, Influence of the management strategy and operating conditions on the performance of an adsorption chiller, Energy, 36 (2011) 5532-5538.
[23] B. Dawoud, P. Hofle, S. Chmielewski, Experimental Investigation of the Effect Of Zeolite Coating Thickness on the Performance of a Novel Zeolite-Water Adsorption Heat Pump Module, Tenth International Conference Enhanced Building Operations, Kuwait (2010).
[24] M. Tatlier, G. Munz, G. Fueldner, S.K. Henninger, Effect of zeolite A coating thickness on adsorption kinetics for heat pump applications, Microporous and Mesoporous Materials, 193 (2014) 115-121.
[25] G. Zhang, D.C. Wang, J.P. Zhang, Y.P. Han, W. Sun, Simulation of operating characteristics of the silica gel–water adsorption chiller powered by solar energy, Solar Energy, 85 (2011) 1469-1478.
[26] H.T. Chua, K.C. Ng, W. Wang, C. Yap, X.L. Wang, Transient modeling of a two-bed silica gel–water adsorption chiller, International Journal of Heat and Mass Transfer, 47 (2004) 659-669.
[27] Y.I. Aristov, A. Sapienza, D.S. Ovoshchnikov, A. Freni, G. Restuccia, Reallocation of adsorption and desorption times for optimisation of cooling cycles, International Journal of Refrigeration, 35 (2012) 525-531.
[28] A. Pesaran, H. Lee, Y. Hwang, R. Radermacher, H.-H. Chun, Review article: Numerical simulation of adsorption heat pumps, Energy, 100 (2016) 310-320.
[29] M. Verde, K. Harby, R. de Boer, J.M. Corberán, Performance evaluation of a waste-heat driven adsorption system for automotive air-conditioning: Part II - Performance optimization under different real driving conditions, Energy, 115 (2016) 996-1009.
[30] S. Narayanan, S. Yang, H. Kim, E.N. Wang, Optimization of adsorption processes for climate control and thermal energy storage, International Journal of Heat and Mass Transfer, 77 (2014) 288-300.
[31] G.H.W. van Benthem, G. Cacciola, G. Restuccia, Regenerative adsorption heat pumps: Optimization of the design, Heat Recovery Systems and CHP, 15 (1995) 531-544.
[32] M. Verde, K. Harby, J.M. Corberán, Optimization of thermal design and geometrical parameters of a flat tube-fin adsorbent bed for automobile air-conditioning, Applied Thermal Engineering, 111 (2017) 489-502.
[33] F. Lanzerath, U. Bau, J. Seiler, A. Bardow, Optimal design of adsorption chillers based on a validated dynamic object-oriented model, Science and Technology for the Built Environment, 21 (2015) 248-257.
[34] M. Gräber, C. Kirches, H.G. Bock, J.P. Schlöder, W. Tegethoff, J. Köhler, Determining the optimum cyclic operation of adsorption chillers by a direct method for periodic optimal control, International Journal of Refrigeration, 34 (2011) 902-913.
[35] A.M. Rivero-Pacho, R.E. Critoph, S.J. Metcalf, Modelling and development of a generator for a domestic gas-fired carbon-ammonia adsorption heat pump, Renewable Energy, 110 (2017) 180-185.
[36] Y.I. Aristov, I.S. Glaznev, I.S. Girnik, Optimization of adsorption dynamics in adsorptive chillers: Loose grains configuration, Energy, 46 (2012) 484-492.
[37] I.S. Girnik, A.D. Grekova, L.G. Gordeeva, Y.I. Aristov, Dynamic optimization of adsorptive chillers: Compact layer vs. bed of loose grains, Applied Thermal Engineering, 125 (2017) 823-829.

[38] A. Sapienza, I.S. Glaznev, S. Santamaria, A. Freni, Y.I. Aristov, Adsorption chilling driven by low temperature heat: New adsorbent and cycle optimization, Applied Thermal Engineering, 32 (2012) 141-146.
[39] J.-Y. San, F.-K. Tsai, Testing of a lab-scale four-bed adsorption heat pump, Applied Thermal Engineering, 70 (2014) 274-281.
[40] S. Graf, F. Lanzerath, A. Sapienza, A. Frazzica, A. Freni, A. Bardow, Prediction of SCP and COP for adsorption heat pumps and chillers by combining the large-temperature-jump method and dynamic modeling, Applied Thermal Engineering, 98 (2016) 900-909.
[41] A. Frazzica, G. Füldner, A. Sapienza, A. Freni, L. Schnabel, Experimental and theoretical analysis of the kinetic performance of an adsorbent coating composition for use in adsorption chillers and heat pumps, Applied Thermal Engineering, 73 (2014) 1022-1031.
[42] S.W. Hong, S.H. Ahn, O.K. Kwon, J.D. Chung, Optimization of a fin-tube type adsorption chiller by design of experiment, International Journal of Refrigeration, 49 (2015) 49-56.
[43] J.P.S. Aniceto, S.P. Cardoso, C.M. Silva, General optimization strategy of simulated moving bed units through design of experiments and response surface methodologies, Computers & Chemical Engineering, 90 (2016) 161-170.
[44] R.M.A. Domingues, M.M.R. de Melo, E.L.G. Oliveira, C.P. Neto, A.J.D. Silvestre, C.M. Silva, Optimization of the supercritical fluid extraction of triterpenic acids from Eucalyptus globulus bark using experimental design, The Journal of Supercritical Fluids, 74 (2013) 105-114.
[45] A.W. Zularisam, A.F. Ismail, M.R. Salim, M. Sakinah, T. Matsuura, Application of coagulation–ultrafiltration hybrid process for drinking water treatment: Optimization of operating conditions using experimental design, Separation and Purification Technology, 65 (2009) 193-210.
[46] M.V. Ponte, L.P. Rivoira, J. Cussa, M.L. Martínez, A.R. Beltramone, O.A. Anunziata, Optimization of the synthesis of SBA-3 mesoporous materials by experimental design, Microporous and Mesoporous Materials, 227 (2016) 9-15.
[47] A. Freni, G. Maggio, S. Vasta, G. Santori, F. Polonara, G. Restuccia, Optimization of a solar-powered adsorptive ice-maker by a mathematical method, Solar Energy, 82 (2008) 965-976.
[48] Y. He, Rapid thermal conductivity measurement with a hot disk sensor: Part 1. Theoretical considerations, Thermochimica Acta, 436 (2005) 122-129.
[49] U. Wittstadt, G. Füldner, V. S., R. Volmer, P. Bendix, L. Schnabel, W. Mittelbach, Adsorption Heat Pumps and Chillers – Recent Developments for Materials and Component, 12th IEA Heat Pump Conference, Rotterdam (2017).
[50] L. Marletta, G. Maggio, A. Freni, M. Ingrasciotta, G. Restuccia, A non-uniform temperature non-uniform pressure dynamic model of heat and mass transfer in compact adsorbent beds, International Journal of Heat and Mass Transfer, 45 (2002) 3321-3330.
[51] J.P.S. Aniceto, C.M. Silva, Preparative Chromatography: batch and continuous, in: Analytical Separation Science, Vol. 4, Wiley, Germany, 2015.
[52] S. Sircar, Linear-driving-force model for non-isothermal gas adsorption kinetics, Journal of the Chemical Society, Faraday Transactions 1: Physical Chemistry in Condensed Phases, 79 (1983) 785-796.
[53] E. Glueckauf, Theory of chromatography. Part 10 – Formulae for diffusion into spheres and their application to chromatography, Trans. Faraday Soc., 51 (1955) 1540-1551.
[54] J.P.S. Aniceto, C.M. Silva, Simulated Moving Bed Strategies and Designs: From Established Systems to the Latest Developments, Separation & Purification Reviews, 44 (2015) 41-73.
[55] B. Mette, H. Kerskes, H. Drück, H. Müller-Steinhagen, Experimental and numerical investigations on the water vapor adsorption isotherms and kinetics of binderless zeolite 13X, International Journal of Heat and Mass Transfer, 71 (2014) 555-561.
[56] M.F. de Lange, K.J.F.M. Verouden, T.J.H. Vlugt, J. Gascon, F. Kapteijn, Adsorption-Driven Heat Pumps: The Potential of Metal–Organic Frameworks, Chemical Reviews, 115 (2015) 12205-12250.

[57] M. Tatlıer, A. Erdem-Şenatalar, Effects of metal mass on the performance of adsorption heat pumps utilizing zeolite 4A coatings synthesized on heat exchanger tubes, International Journal of Refrigeration, 23 (2000) 260-268.
[58] D.C. Montgomery, Design and Analysis of Experiments, eight ed., John Wiley & Sons Inc, New Jersey, 2012.
[59] K. Schumann, B. Unger, A. Brandt, F. Scheffler, Investigation on the pore structure of binderless zeolite 13× shapes, Microporous and Mesoporous Materials, 154 (2012) 119-123.
[60] İ. Solmuş, C. Yamalı, B. Kaftanoğlu, D. Baker, A. Çağlar, Adsorption properties of a natural zeolite–water pair for use in adsorption cooling cycles, Applied Energy, 87 (2010) 2062-2067.
[61] Grace Davison Sylobead adsorbents for process applications, Molecular sieves and silica gel. https://grace.com/general-industrial/en-us/Documents/sylobead_br_E_2010_f100222_web.pdf, 2010 (accessed 20.01.2017).
[62] Y. Liu, K.C. Leong, The effect of operating conditions on the performance of zeolite/water adsorption cooling systems, Applied Thermal Engineering, 25 (2005) 1403-1418.
[63] J. Jänchen, H. Stach, Shaping adsorption properties of nano-porous molecular sieves for solar thermal energy storage and heat pump applications, Solar Energy, 104 (2014) 16-18.
[64] C. Lehmann, S. Beckert, R. Gläser, O. Kolditz, T. Nagel, Assessment of adsorbate density models for numerical simulations of zeolite-based heat storage applications, Applied Energy, 185, Part 2 (2017) 1965-1970.
[65] P. Malbrunot, D. Vidal, J. Vermesse, R. Chahine, T.K. Bose, Adsorbent Helium Density Measurement and Its Effect on Adsorption Isotherms at High Pressure, Langmuir, 13 (1997) 539-544.
[66] D.B. Riffel, U. Wittstadt, F.P. Schmidt, T. Núñez, F.A. Belo, A.P.F. Leite, F. Ziegler, Transient modeling of an adsorber using finned-tube heat exchanger, International Journal of Heat and Mass Transfer, 53 (2010) 1473-1482.
[67] P. Tatsidjodoung, N. Le Pierrès, J. Heintz, D. Lagre, L. Luo, F. Durier, Experimental and numerical investigations of a zeolite 13X/water reactor for solar heat storage in buildings, Energy Conversion and Management, 108 (2016) 488-500.
[68] L. Qiu, Thermal Properties of Framework Materials: Selected Zeolites, Clathrates and an Organic Diol, PhD thesis, Dalhousie University, Canada, 2000.
[69] M. Winterberg, E. Tsotas, Correlations for effective heat transport coefficients in beds packed with cylindrical particles, Chemical engineering science, 55 (2000) 5937-5943.
[70] A. Freni, B. Dawoud, L. Bonaccorsi, S. Chmielewski, A. Frazzica, L. Calabrese, G. Restuccia, Characterization of Zeolite-based Coatings for Adsorption Heat Pumps, Springer, New York, 2015.
[71] L. Bonaccorsi, L. Calabrese, A. Freni, E. Proverbio, G. Restuccia, Zeolites direct synthesis on heat exchangers for adsorption heat pumps, Applied Thermal Engineering, 50 (2013) 1590-1595.

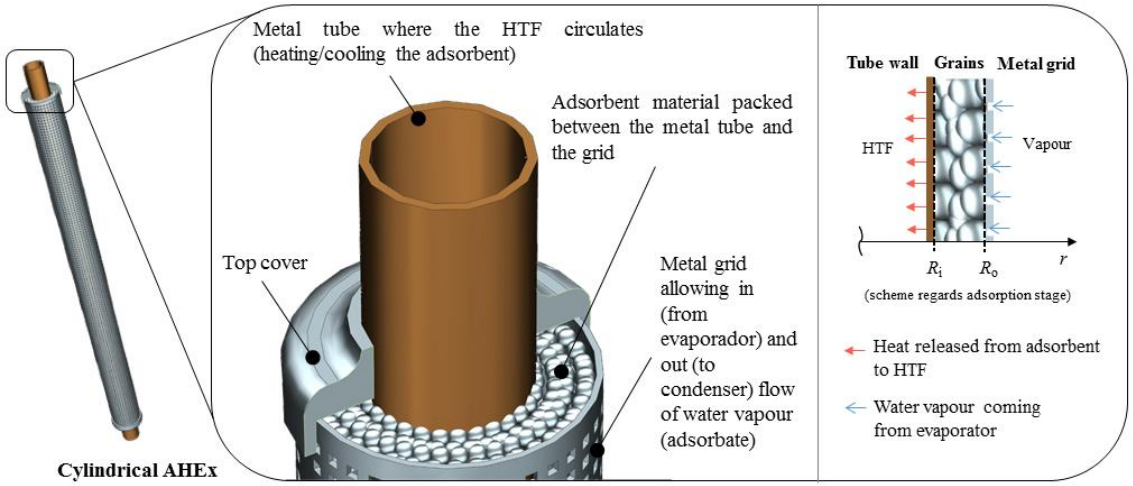

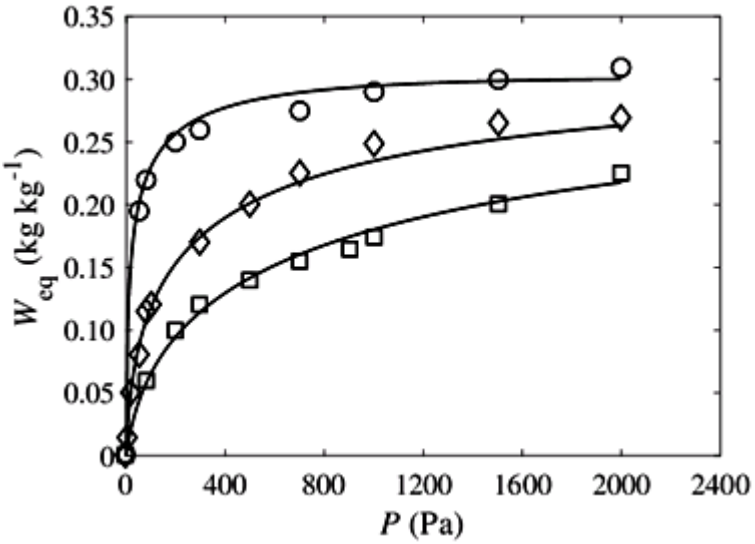

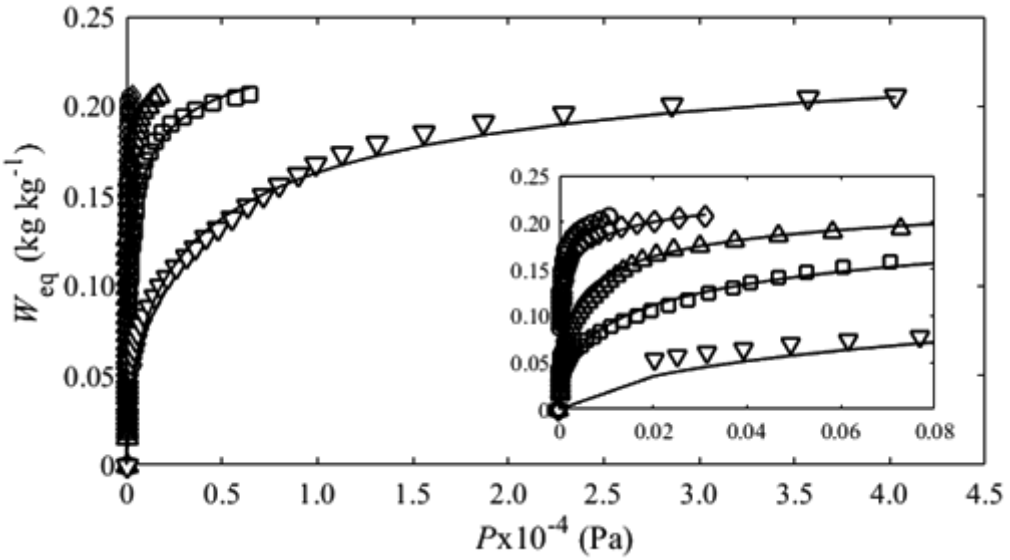

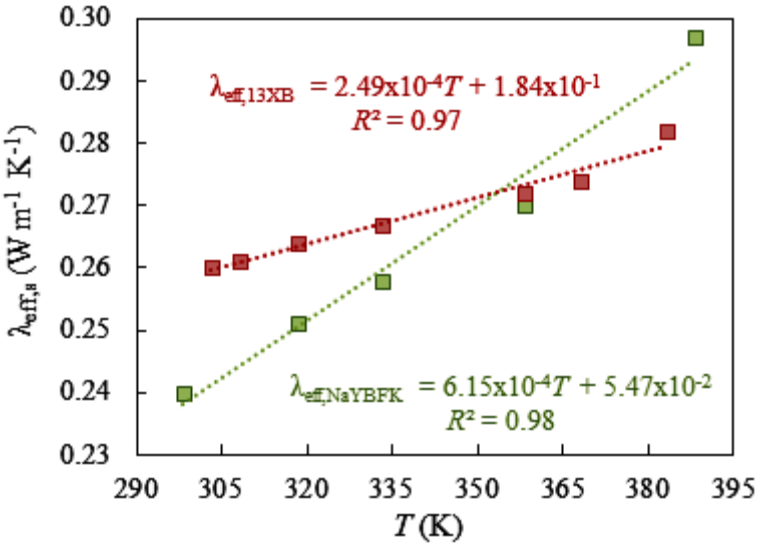

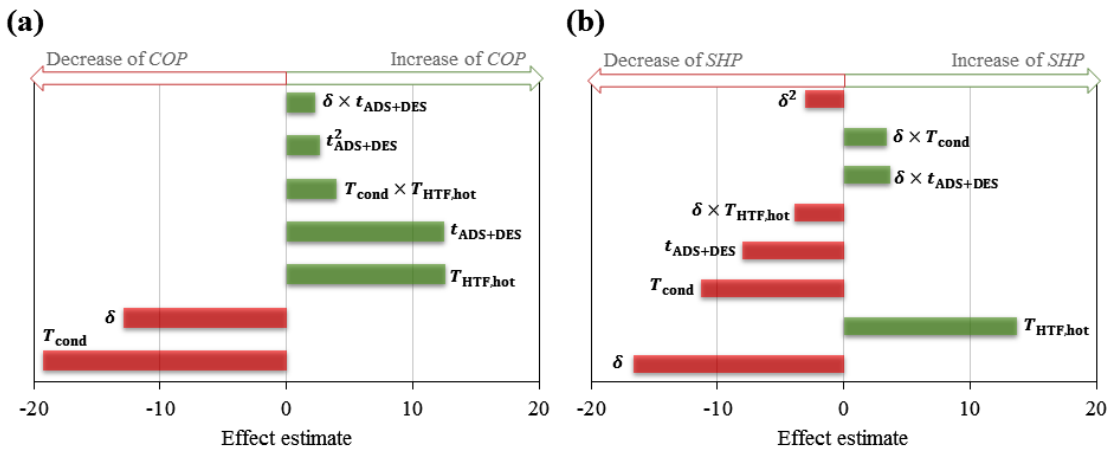

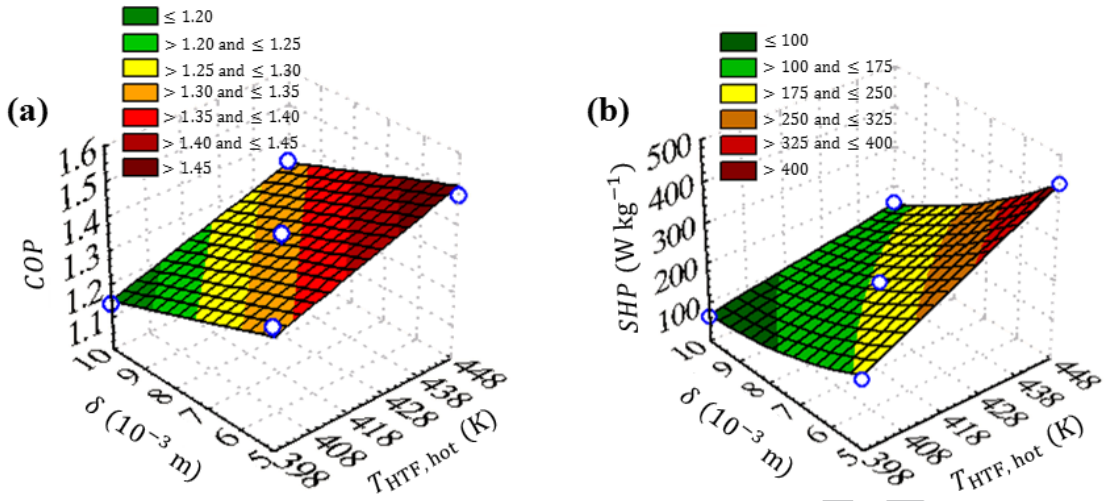

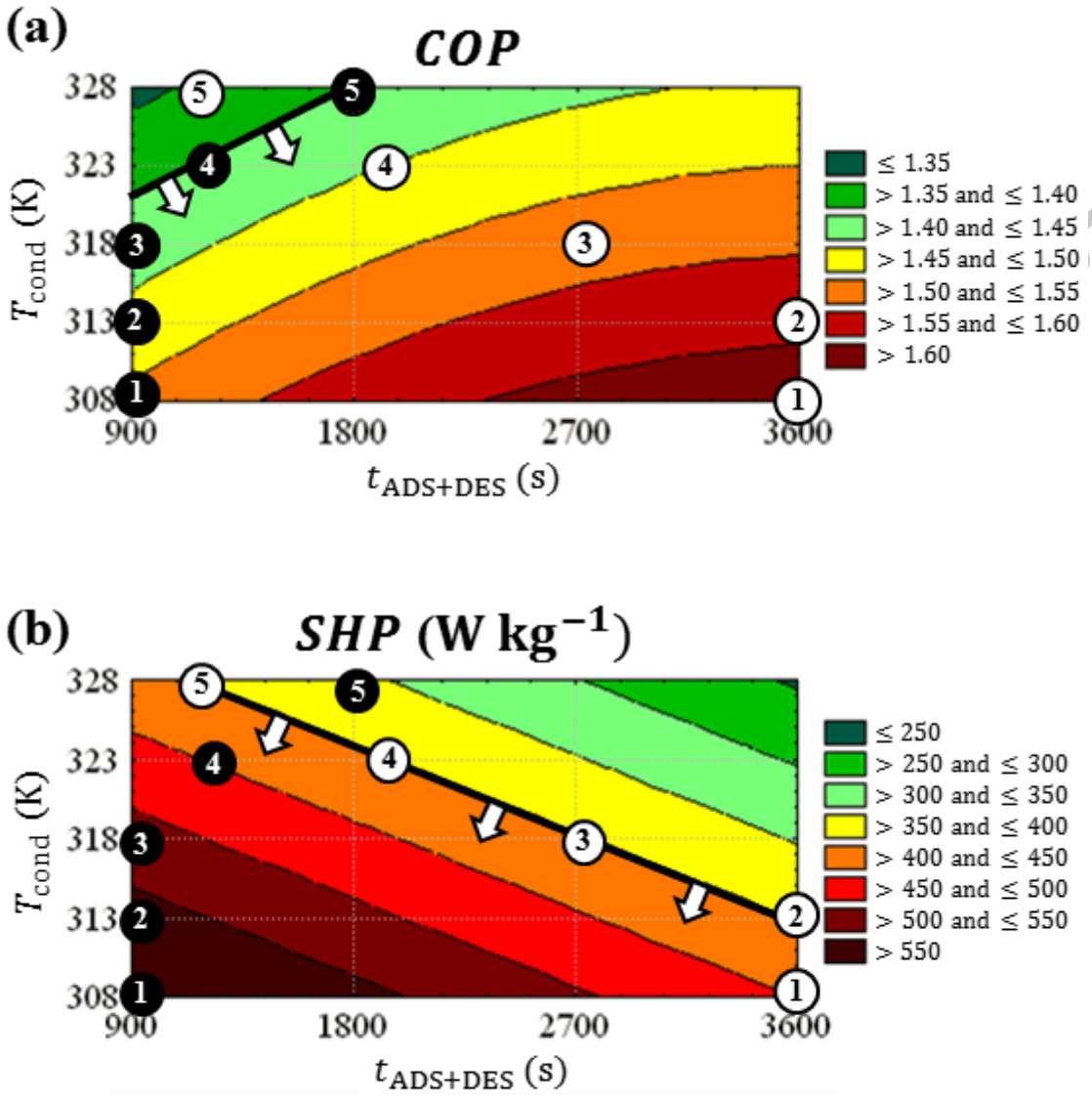
(a)
COP
328
323
318
313
308
$T_{cond}$ (K)
900
1800
2700
3600
$t_{ADS+DES}$ (s)
≤ 1.35
> 1.35 and ≤ 1.40
> 1.40 and ≤ 1.45
> 1.45 and ≤ 1.50
> 1.50 and ≤ 1.55
> 1.55 and ≤ 1.60
> 1.60
(b)
SHP (W kg$^{-1}$)
328
323
318
313
308
$T_{cond}$ (K)
900
1800
2700
3600
$t_{ADS+DES}$ (s)
≤ 250
> 250 and ≤ 300
> 300 and ≤ 350
> 350 and ≤ 400
> 400 and ≤ 450
> 450 and ≤ 500
> 500 and ≤ 550
> 550
SHP maximization
COP maximization

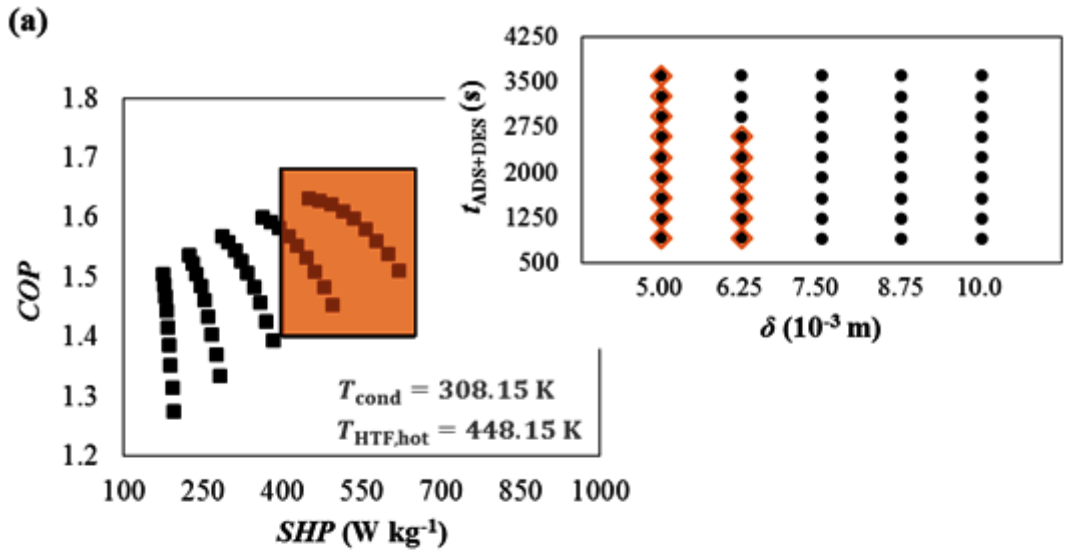
(a)
COP
SHP (W kg-1)
tADS+DES (s)
δ (10-3 m)
Tcond = 308.15 K
THTF,hot = 448.15 K

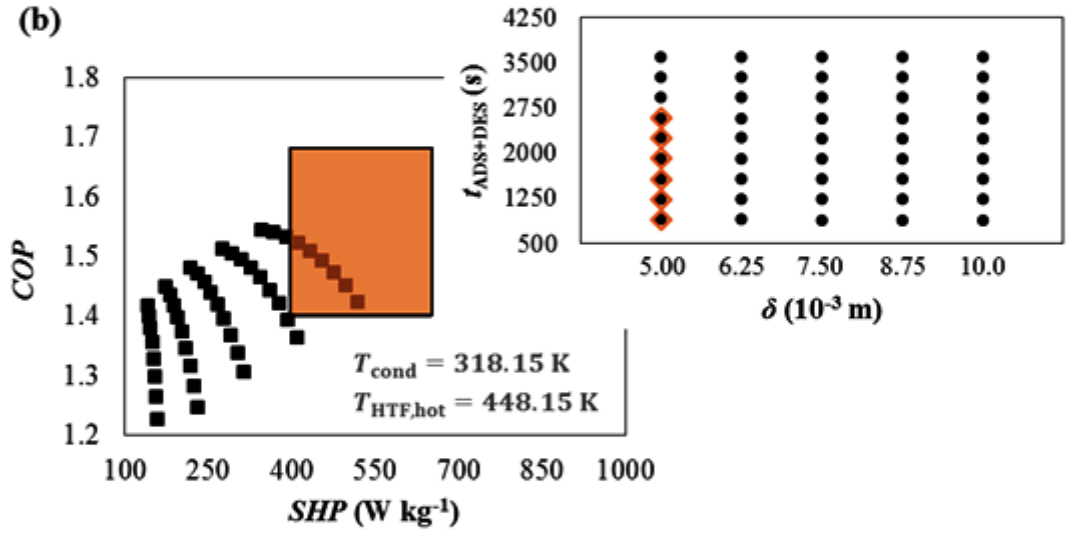
(b)
COP
SHP (W kg-1)
tADS+DES (s)
δ (10-3 m)
Tcond = 318.15 K
THTF,hot = 448.15 K

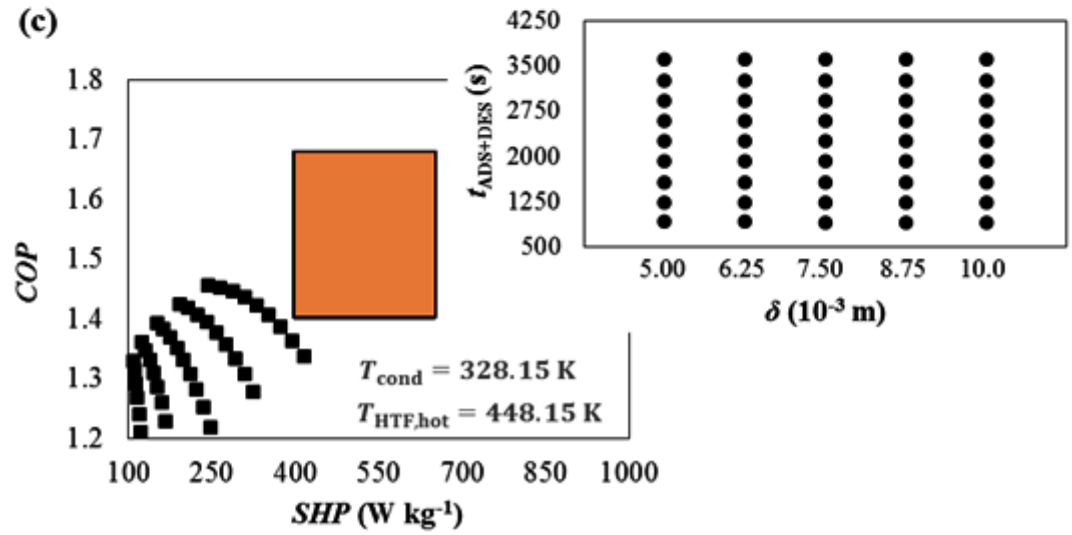
(c)
COP
SHP (W kg-1)
tADS+DES (s)
δ (10-3 m)
Tcond = 328.15 K
THTF,hot = 448.15 K

Table 1 - Factors, levels and codification considered for the Box-Behnken design.

| **Factor** | **Level** | | |
|---|---|---|---|
| | Low (-1) | Medium (0) | High (+1) |
| $t_{\mathrm{ADS+DES}}$ (s) [(a)] | 900 (15 min) | 2250 (37.5 min) | 3600 (60 min) |
| $T_{\mathrm{cond}}$ (K) | 308.15 | 318.15 | 328.15 |
| $T_{\mathrm{HTF,hot}}$ (K) | 398.15 | 423.15 | 448.15 |
| $\delta$ (m) | $5\times10^{-3}$ | $7.5\times10^{-3}$ | $10\times10^{-3}$ |

[(a)] Isobaric adsorption and desorption are the longest stages, therefore $t_{\mathrm{ADS+DES}}$ is similar to $t_{\mathrm{cycle}}$.

Table 2 - Dubinin-Astakhov (DA) isotherms of water vapour on 13XBFK, NaYBFK and 13XB, and expressions for the linear driving force (LDF) global coefficient ($\boldsymbol{K_{LDF}}$).

| **Description** | **Equation** | **Eq.** |
|---|---|---|
| 13XBFK/water isotherm (DA model) [a,b] | $W_{eq} = 3.4103 \times 10^{-4} \rho_a \, exp\left[-\left(\frac{\Re T}{1.1923 \times 10^6 M} ln\frac{P_{sat}}{P}\right)^{1.55}\right]$, where $\rho_a = \frac{\rho_{water,293.15\ K}}{1+\beta_{water,293.15\ K}(T-293.15)}$ | (11) |
| NaYBFK/water isotherm (DA model) | $W_{eq} = 0.301 \, exp\left[-2.62 \times 10^{-8}\left(Tln\frac{P_{sat}}{P}\right)^{2.33}\right]$ | (12) |
| 13XB /water isotherm (DA model) | $W_{eq} = 0.231 \, exp\left[-6.28 \times 10^{-9}\left(Tln\frac{P_{sat}}{P}\right)^{2.41}\right]$ | (13) |
| Linear driving force (LDF) global mass transfer coefficient [c] | $K_{LDF} = \frac{\Omega D_{eff}}{R_p^2 H}$, where $\Omega = 15$ (for spheres), $D_{eff} = \frac{\varepsilon_p}{\tau_p}\left(\frac{1}{D_K} + \frac{1}{D_m}\right)^{-1}$ and $H = \rho_p \frac{\Re T}{M}\frac{\partial W_{eq}}{\partial P}$ | (14) |

[a] The $\boldsymbol{\beta_{water,293.15\ K}}$ is the thermal expansion coefficient of water at 293.15 K, which is 2.07x10$^{-4}$ K$^{-1}$ according with the Mugele model reported in Fig. 1(b) of ref. [64]. [b] The maximum loading ($\boldsymbol{W_0}$) corresponds to the term $\boldsymbol{3.4103 \times 10^{-4} \rho_a}$ (in kg kg$^{-1}$). [c] The equations for $\boldsymbol{D_K}$ and $\boldsymbol{D_m}$ are given in Supplementary Information (Section 2.2).

Table 3 - Main properties of the adsorbents, bed dimensions and operating conditions considered in the simulations.

| | **NaYBFK** | **Ref.** | **13XBFK** | **Ref.** | **13XB** | **Ref.** |
|---|---|---|---|---|---|---|
| $C_{p,s}$ (J kg$^{-1}$ K$^{-1}$) | 855 – 898 [(a)] | [68] | 880 | [55] | 910 – 945 [(a)] | [68] |
| $\lambda_{eff,s}$ (W m$^{-1}$ K$^{-1}$) | 0.272 – 0.293 [(a)] | This work | 0.24 [(b)] | | 0.272 – 0.281 [(a)] | This work |
| $Q_{ads}$ (J kg$^{-1}$) | 3.05 × 10$^6$ [(a)] | | 3.50 × 10$^6$ [(a)] | | 3.34 × 10$^6$ [(a)] | |
| $\rho_s$ (kg m$^{-3}$) | 2475 [(a)] | | 2875 [(c)] | This work | 2447 [(a)] | |
| $\rho_p$ (kg m$^{-3}$) | 1117 [(a)] | | 1150 | | 1117 [(a)] | |
| $\varepsilon_p$ | 0.55 [(a)] | | 0.60 | [55] | 0.54 [(a)] | |
| $\tau_p$ | 3.8 [(a)] | | 4.0 | | 3.9 [(a)] | |
| $d_p$ (m) | 0.5 x 10$^{-3}$ | | | | | |
| $\varepsilon_b$ | 0.40 [(d)] | | | | | |
| *Adsorbent bed dimensions and operating conditions* | | | | | | |
| $R_i$ (m) | 7.5 x 10$^{-3}$ | | | | | |
| $T_{evap}$ (K); $P_{evap}$ (Pa) | 278.15; 870 | | | | | |
| $T_{HTF,cool}$ (K) [(e)] | 308.15 – 328.15 | | | | | |

[(a)] Details given in the Supplementary Information (Section 2).

[(b)] Obtained considering $\lambda_{eff,s} = \lambda_s(1 - \varepsilon_b)$, using $\lambda_s = 0.4$ W m$^{-1}$ K$^{-1}$ as reported in ref. [55].

[(c)] Calculated using data reported in ref. [55] for particle density ($\rho_p$) and porosity ($\varepsilon_p$) of 1150 kg m$^{-3}$ and 0.6, respectively, as follows: $\rho_s = \frac{\rho_p}{(1-\varepsilon_p)}$.

[(d)] The porosity of undisturbed random beds of spheres normally lies between 0.36-0.42, as reported in ref. [69].

[(e)] $T_{HTF,cool}$ was coincident with $T_{cond}$.

Table 4 - Box-Behnken design matrix of four factors ($t_{ADS+DES}$, $T_{cond}$, $T_{HTF,hot}$, $\delta$) and three levels, and results of *COP* and *SHP* for NaYBFK, 13XBFK and 13XB beds.

| Run | $t_{ADS+DES}$ (s) [a] | $T_{cond}$ (K) [a] | $T_{HTF,hot}$ (K) [a] | $\delta$ (m) [a] | NaYBFK | | 13XBFK | | 13XB | |
|---|---|---|---|---|---|---|---|---|---|---|
| | | | | | *COP* | *SHP* (W kg$^{-1}$) | *COP* | *SHP* (W kg$^{-1}$) | *COP* | *SHP* (W kg$^{-1}$) |
| 1 | 900 (-1) | 308.15 (-1) | 423.15 (0) | 7.5x10$^{-3}$ (0) | 1.38 | 322 | 1.26 | 238 | 1.27 | 248 |
| 2 | 3600 (1) | 308.15 (-1) | 423.15 (0) | 7.5x10$^{-3}$ (0) | 1.51 | 201 | 1.38 | 150 | 1.38 | 150 |
| 3 | 900 (-1) | 328.15 (1) | 423.15 (0) | 7.5x10$^{-3}$ (0) | 1.05 | 141 | 1.00 | 105 | 1.06 | 129 |
| 4 | 3600 (1) | 328.15 (1) | 423.15 (0) | 7.5x10$^{-3}$ (0) | 1.26 | 95 | 1.18 | 76 | 1.19 | 76 |
| 5 | 900 (-1) | 318.15 (0) | 398.15 (-1) | 7.5x10$^{-3}$ (0) | 1.10 | 128 | 1.05 | 102 | 1.08 | 113 |
| 6 | 3600 (1) | 318.15 (0) | 398.15 (-1) | 7.5x10$^{-3}$ (0) | 1.32 | 87 | 1.21 | 72 | 1.19 | 79 |
| 7 | 900 (-1) | 318.15 (0) | 448.15 (1) | 7.5x10$^{-3}$ (0) | 1.31 | 333 | 1.20 | 245 | 1.21 | 265 |
| 8 | 3600 (1) | 318.15 (0) | 448.15 (1) | 7.5x10$^{-3}$ (0) | 1.47 | 220 | 1.33 | 153 | 1.37 | 164 |
| 9 | 2250 (0) | 308.15 (-1) | 398.15 (-1) | 7.5x10$^{-3}$ (0) | 1.41 | 159 | 1.30 | 124 | 1.30 | 126 |
| 10 | 2250 (0) | 328.15 (1) | 398.15 (-1) | 7.5x10$^{-3}$ (0) | 1.05 | 48 | 1.01 | 40 | 1.09 | 47 |
| 11 | 2250 (0) | 308.15 (-1) | 448.15 (1) | 7.5x10$^{-3}$ (0) | 1.51 | 308 | 1.38 | 223 | 1.39 | 247 |
| 12 | 2250 (0) | 328.15 (1) | 448.15 (1) | 7.5x10$^{-3}$ (0) | 1.34 | 196 | 1.17 | 138 | 1.25 | 155 |
| 13 | 2250 (0) | 318.15 (0) | 423.15 (0) | 7.5x10$^{-3}$ (0) | 1.36 | 171 | 1.23 | 129 | 1.26 | 139 |
| 14 | 2250 (0) | 308.15 (-1) | 423.15 (0) | 10x10$^{-3}$ (1) | 1.40 | 148 | 1.27 | 110 | 1.29 | 118 |
| 15 | 2250 (0) | 328.15 (1) | 423.15 (0) | 10x10$^{-3}$ (1) | 1.10 | 68 | 1.03 | 52 | 1.07 | 62 |
| 16 | 3600 (1) | 318.15 (0) | 423.15 (0) | 10x10$^{-3}$ (1) | 1.34 | 91 | 1.21 | 70 | 1.24 | 78 |
| 17 | 900 (-1) | 318.15 (0) | 423.15 (0) | 10x10$^{-3}$ (1) | 1.12 | 142 | 1.04 | 105 | 1.07 | 111 |
| 18 | 2250 (0) | 318.15 (0) | 448.15 (1) | 10x10$^{-3}$ (1) | 1.33 | 154 | 1.22 | 113 | 1.24 | 127 |
| 19 | 2250 (0) | 318.15 (0) | 398.15 (-1) | 10x10$^{-3}$ (1) | 1.14 | 62 | 1.06 | 50 | 1.13 | 56 |
| 20 | 2250 (0) | 318.15 (0) | 398.15 (-1) | 5x10$^{-3}$ (-1) | 1.36 | 176 | 1.26 | 146 | 1.24 | 124 |
| 21 | 2250 (0) | 318.15 (0) | 448.15 (1) | 5x10$^{-3}$ (-1) | 1.48 | 431 | 1.35 | 318 | 1.36 | 304 |
| 22 | 900 (-1) | 318.15 (0) | 423.15 (0) | 5x10$^{-3}$ (-1) | 1.36 | 427 | 1.24 | 322 | 1.26 | 344 |
| 23 | 3600 (1) | 318.15 (0) | 423.15 (0) | 5x10$^{-3}$ (-1) | 1.47 | 224 | 1.36 | 177 | 1.33 | 136 |
| 24 | 2250 (0) | 308.15 (-1) | 423.15 (0) | 5x10$^{-3}$ (-1) | 1.53 | 412 | 1.41 | 311 | 1.39 | 275 |
| 25 | 2250 (0) | 328.15 (1) | 423.15 (0) | 5x10$^{-3}$ (-1) | 1.32 | 192 | 1.22 | 155 | 1.22 | 137 |

[a] Values inside parenthesis are the codified levels of each variable under the context of DoE.

## Highlights

- Study of X and Y zeolites with/without binder for adsorption heat pumps (AHPs)
- Results from Box-Behnken design and response surface methodology (DoE/RSM) analyzed
- Studied variables: bed thickness, time, condenser and heat source temperatures
- The binder in the 13X formulation does not penalize AHP performance significantly
- DoE/RSM aid efficient optimization of AHP design and control

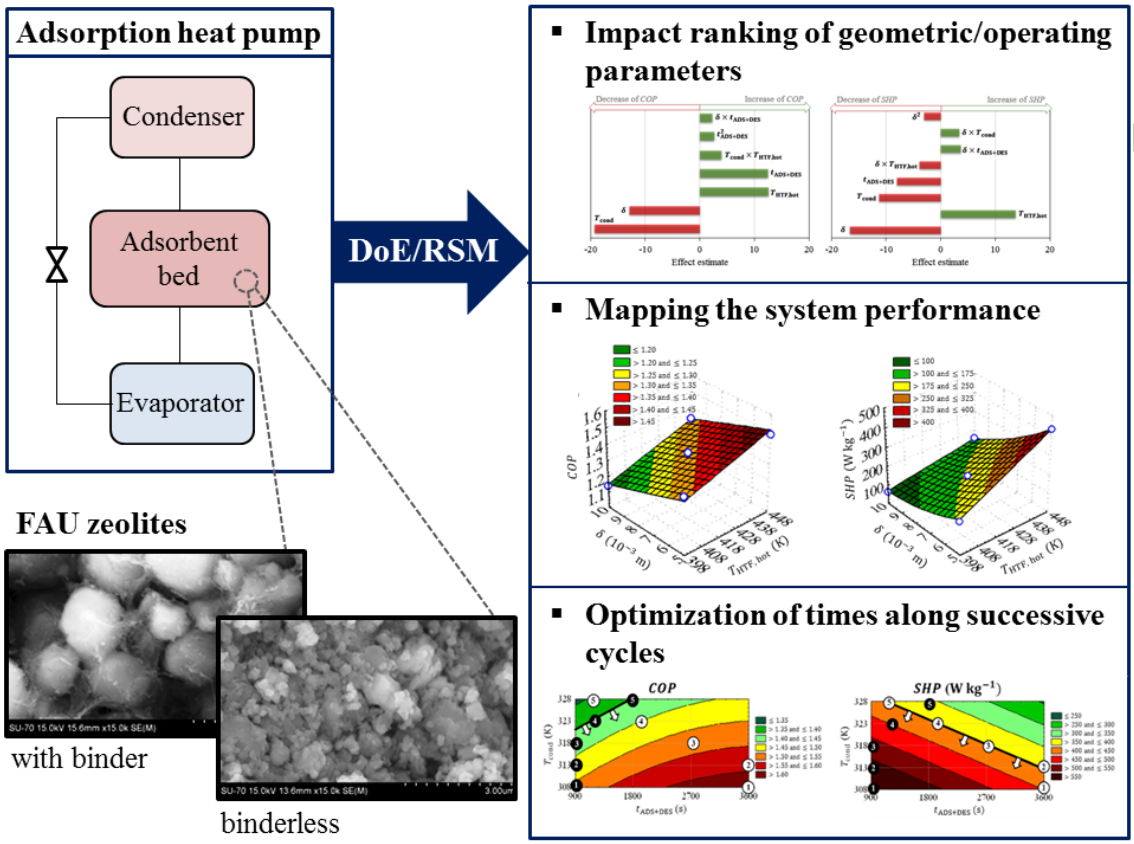
Adsorption heat pump
Condenser
Adsorbent bed
Evaporator
DoE/RSM
FAU zeolites
with binder
binderless
Impact ranking of geometric/operating parameters
Mapping the system performance
Optimization of times along successive cycles
COP
SHP (W kg⁻¹)